NASA Technical Memorandum 81220

Two-Photon Excitation of Nitric Oxide Fluorescence as a Temperature Indicator in Unsteady Gas-Dynamic Processes

R. L. McKenzie and K. P. Gross

September 1980

National Aeronautics and Space Administration

NASA Technical Memorandum 81220

Two-Photon Excitation of Nitric Oxide Fluorescence as a Temperature Indicator in Unsteady Gas-Dynamic Processes

R. L. McKenzie, Ames Research Center, Moffett Field, California
K. P. Gross, Polyatomics Research, Inc., Mountain View, California

NASA
National Aeronautics and
Space Administration

Ames Research Center
Moffett Field, California 94035

Abstract

A laser-induced fluorescence technique, which is especially suitable for measuring fluctuating temperatures in cold turbulent flows containing very low concentrations of nitric oxide, is described and analyzed. Temperatures below 300 K may be resolved with signal-to-noise ratios greater than 50:1, using commercially available, high-peak-power, tunable dye lasers. The method relies on the two-photon excitation of selected ro-vibronic transitions in the $NO(A^2\Sigma^+, v' = 0 \leftarrow X^2\Pi, v'' = 0)$ γ-band. The analysis includes the effects of fluorescence quenching and shows the technique to be effective at all densities below ambient. Signal-to-noise ratio estimates are based on a preliminary measurement of the two-photon absorptivity for a selected rotational transition in the NO $\gamma(0,0)$ band.

I. Introduction

The spectroscopic measurement of temperature fluctuations with adequate temporal and spatial resolution in unsteady gas dynamics processes has been an elusive objective in spite of the dependence of many spectroscopic features on the sample temperature. Modern reviews of the subject[1-3] offer no suitable techniques for unsteady environments regardless of whether they are considering low-temperature turbulent flows or high-temperature combustion. The absence of practical techniques persists for a variety of underlying reasons. Typically, older methods, such as optical pyrometry, absorption, and line-reversal spectroscopy,[2] are all spatially averaged techniques (along the line of sight) and, thus, are of limited usefulness even when they can be implemented with high-frequency response. Modern methods include electron-beam fluorescence,[3,4] laser Raman scattering,[1,5] coherent wave mixing,[6] and laser-induced fluorescence[7]; but most of these techniques also have limited application in unsteady environments. For example, electron-beam fluorescence has been applied successfully at low densities where electron scattering and fluorescence quenching are minimized, but few unsteady flow processes of interest occur at low densities. Laser Raman scattering is best applied at high densities, but its application has been restricted by the very small Raman scattering cross sections.

Consequently, signal averaging is often required to obtain adequate measurement accuracy at the expense of temporal information.

Without signal averaging, the increased laser intensities required to produce scattering signals in excess of the unavoidable photon-statistical noise generally exceed the limits imposed by electric breakdown.[8] In addition, most techniques for resolving the Raman spectrum are sensitive to temperature variations only at mean values greater than 500 K, making the method interesting for hot combustion environments at very high densities, but not for cold turbulent flows typical of fluid mechanical studies.

Two recently developed approaches that, at first, appear promising for practical temperature measurements in unsteady environments are those based on coherent anti-Stokes Raman scattering (CARS)[6] and a variety of methods using laser-induced fluorescence (e.g., Ref. 7). However, all of the specific techniques known to us that have been demonstrated or proposed to date allow the discrimination of temperature variations only for mean values greater than 1000 K, principally because they seek to maximize signal levels by using low spectral resolution. The results are then sensitive only to vibrational band shape and are limited to temperatures of the order of the characteristic vibrational temperature, $\hbar\omega_e/k$, where ω_e is the vibrational constant of the molecule being probed. Coherent wave mixing techniques[6] suffer added difficulties due to the practical aspects of producing and maintaining two or more coherently correlated high-power laser beams and the associated signal noise induced by their uncorrelated mixing.

Applications of laser-induced fluorescence also require careful consideration of some fundamental aspects. Those of primary importance include: (1) the provision of a molecular species with excitation and fluorescence transitions of sufficient strength and suitable accessibility to available laser frequencies; (2) the method of resolving spectral features with sufficient detail and freedom of noise or scattered light to accurately infer a temperature; and (3) an accounting of the effects of fluorescence quenching and radiative trapping in a manner that unambiguously allows temperature and density fluctuations to be isolated from one another and the results to be simply interpreted. The difficulty in achieving all of these criteria often discourage the use of seemingly attractive fluorescence schemes in an unsteady environment.

Our interest has been centered primarily on the measurement of fluctuating temperatures in cold turbulent flows, an application excluded by even the most feasible methods described above because of the low temperatures typically involved. Usually, such flows are produced in unheated wind tunnels where a high-density gas expands from ambient temperatures to values as low as 100 K. Sensitive measurements in that range, using spectroscopic methods, demand that rotational line spectra be used because rotational energy differences are typically in the range, $\hbar B_e/k \simeq 2$ to 80 K, where B_e is the molecular rotational constant. Fortunately, rotational temperatures can be obtained even in the presence of prominent

quenching by measuring the relative populations of rotational states in the molecular ground vibronic level and using their ratio in the Boltzmann equation. The only implicit assumptions required are that the rotational states being excited are quenched equally and that the ground-state rotational populations are at local thermodynamic equilibrium in the sampling volume. These assumptions are justified in most cases by noting first that the dependence of quenching on rotational quantum number is usually small.[9,10] However, careful consideration must be given to those molecules with the smaller ratios of the fundamental vibrational and rotational constants, ω_e/B_e (e.g., H_2).[11] Second, one can show that molecular rotation may be considered in thermodynamic equilibrium with the bulk mixture at least in all nonreacting flows except the most rapid nozzle expansions to very low densities because, for most molecules, only a few collisions are required for rotational energy transfer.[12]

In this paper, we describe an effective and practical means of measuring relative rotational state populations that depends on the pulsed two-photon excitation of the $NO(A^2\Sigma^+, v' = 0 \leftarrow X^2\Pi, v'' = 0)$ γ-band and its subsequent fluorescence. Nitric oxide is rotationally simple and often a constituent in combustion processes of interest. For cold flows, it may be added as a seed gas in very low concentrations and still provide adequate signals (as we shall show). A second major purpose of this paper, in addition to describing the advantages of two-photon excitation and to analyzing the feasibility

of its use for fluctuating temperature measurements, is to present a pragmatic and unified formulation for quantitatively describing two-photon fluorescence excitation in this application. During the course of these studies, we have encountered a variety of theoretical formulations[13-21] that, while generally correct, are not all unambiguously applied to the experimental conditions at hand. For example, the parameters used to evaluate the two-photon absorptivity of a given medium are given in several forms ranging from the third-order susceptibility (with a disparity of numerical constants) to a cross section per incident photon flux. Because of the variety of analytic approaches and notation, their relationship to one another is not always easily decided. Although this situation is not entirely distinct from that still existing for single-photon interactions, the clearly undesirable aspect of the two-photon absorptivity parameter that appears most frequently in the literature[13] is its implicit dependence on the conditions of the experiment as well as on the molecular properties of the medium. In particular, the effects of laser spectral width are often omitted from the definition of the parameter, leaving its use in a specific application at the risk of the experimentalist. In other cases, not all formulations clearly isolate the possible strong effects of phase coherence in the incident laser radiation. We have attempted to unify these considerations and to define their importance for this application.

In the sections to follow, we first describe the temperature measurement concept and the experimental approach considered to implement it. A formulation for quantitatively analyzing the experiment is then developed from a view in which the constraints on its application are emphasized. The analysis is first applied to the interpretation of a preliminary two-photon absorptivity measurement in NO that provides an absolute measure of the subsequent fluorescence energy produced in a general environment. The results are compared to a literature value obtained with a much different technique.[22] Finally, estimates are made of the anticipated signal-to-noise ratios that may be achieved in low-temperature supersonic flows. The equivalence of our formulation to several others in the literature is defined in the Appendix.

II. Temperature Measurement Concept

Two-photon absorption by $NO(A^2\Sigma^+, v' = 0 \leftarrow X^2\Pi, v'' = 0)$ has been shown to produce easily detected fluorescence from the ultraviolet γ-bands when induced by commercially available tunable dye lasers.[23-28] When compared to its single-photon counterpart, the two-photon spectrum has some useful differences in its rotational line structure, as illustrated in Fig. 1. For example, $\Delta J = \pm 2$ transitions are allowed by two-photon interactions, leading to eight additional rotational branches. Many lines in the outer $S(\Delta J = +2)$ and $O(\Delta J = -2)$ branches are more dispersed and less

overlapped than any in the single-photon spectrum. The isolation of a single rotational transition, using a laser spectral width as large as 0.5 cm^{-1}, is easily accomplished even in the presence of substantial collisional broadening. Similar features are not available for single-photon transitions.[29]

The use of two-photon absorption to obtain a rotational temperature is illustrated in Fig. 2. Two individual transitions originating from different rotational levels of the ground electronic and vibrational state are each induced by single laser pulses tuned to half of their respective transition energies. The required laser wavelengths, near 450 nm, are conveniently obtained. The relative energy absorbed by each transition is measured by monitoring the subsequent broad-band ultraviolet fluorescence in the range from 225 to 300 nm. Spatial resolution is achieved by viewing the emission from only a small volume centered on the focal region of the laser beams. The fluorescence and scattered laser light are easily separated spectrally by a solar blind photomultiplier and a low-pass absorption filter. Since only the ratio of energies absorbed is required, the redistribution of energy among rotational levels of the excited vibronic state and their nonradiative quenching has no effect on the measurement, providing the quenching rates are insensitive to rotational quantum number. Following excitation, the time-integral of the fluorescence signal is proportional to the absorbed energy. Any capacitive integration

by a well designed electronic detection system distorts the time-dependent waveform, but does not change its integral. Thus, ultra-fast photodetection is not necessarily required.

In our concept, fluorescence from each of the two transitions is isolated by separating the two excitation pulses slightly in time. The resulting superimposed waveforms, shown schematically in Fig. 3, can then be recorded with a single photodetection system, digitized, and later deconvolved and integrated. An absolute rotational temperature, T_r, is then obtained through the Boltzmann relation:

$$\int_0^\infty I_1(t)dt \Big/ \int_0^\infty I_2(t)dt \sim \exp[(-\hbar\omega_1 - \hbar\omega_2)/kT_r] \ , \qquad (1)$$

where $I_i(t)$ is the time-dependent fluorescence signal, and $\hbar\omega_i$ is the energy of each transition. The remaining sections of this paper are devoted to evaluating the proportionality constant implied by Eq. (1).

A schematic of the experimental apparatus is shown in Fig. 4. A single Nd-YAG laser, with its output tripled to 355 nm, pumps two grating-tuned dye laser systems. An optical delay separates the dye laser pulses in time. The two dye laser beams are then spatially combined and passed first through a reference cell. The reference-cell signal provides a measure of the pulse-to-pulse variations in signal due to the lasers and allows normalization of the test chamber measurements. Similar reference-cell applications with

nonlinear processes dependent on phase coherence have not been very successful. Its use here emphasizes a distinct advantage of this incoherent fluorescence technique.

III. Theoretical Description

The primary aspects of two-photon absorption have been thoroughly described in the literature,[13-18] including physically precise formulations in terms of the density matrix that account for the effects of coherence, strong fields, and resonant intermediate states.[19-21] In this section, we take a more heuristic view intended only to identify the physical aspects of the process that are important to this application and to qualify the formulation used to describe them. Our considerations shall be limited to cases in which resonant intermediate states do not exist, the field strength is sufficient only to induce two-photon-resonant absorption, and, consequently, the effects of coherence are important only in the phase correlations of the field itself. Our formulation is also specialized to cases in which the duration of the laser pulse is short compared with the fluorescence decay time including the effects of quenching, but long compared with the collisional dephasing time. This condition allows the excitation and decay processes to be decoupled and a rate-equation description of the molecular response to be used. The effects of saturation and finite spectral widths are then introduced in a manner similar to the treatment for single-photon

interactions. The special features of Doppler-free two-photon absorption[17] are not considered because the added experimental complication is not required to achieve the spectral resolution or absorptive coupling necessary in this application. At the higher densities common in wind-tunnel environments, homogeneous line broadening precludes the benefits of Doppler-free spectroscopy entirely. However, the influence of focusing will be considered for a simple example to illustrate its experimental importance.

A. Microscopic Aspects of Two-Photon Absorption

Consider the near-resonant interaction of two-photons with angular frequencies, ω_1 and ω_2, and a molecular system, originally in the lower state $|\ell\rangle$, excited to the upper state $|u\rangle$ where $\hbar\omega_1 + \hbar\omega_2 \simeq E_u - E_\ell$. All other states of the system, with transition energies far from resonance with the radiative field, are represented by the group $|m\rangle$. Ignoring any spectral bandwidths for the moment, two Fourier components of the electric field may be represented classically by

$$\vec{\xi}(\vec{r},t) = \mathrm{Re}[\vec{e}_1\xi_1 e^{-i\omega_1 t} + \vec{e}_2\xi_2 e^{-i\omega_2 t}] \ ,$$

where the unit vectors $\vec{e}_i$ define the polarization of each component and all amplitudes and polarizations are assumed to be slowly varying relative to the instantaneous field. The molecular system as it is driven by the field may then be represented by a time-dependent wave function, $\psi(\vec{r},t)$, with coupling through electric-dipole

interactions. The electric-dipole moment of each field component, $\vec{\mu} = -e\vec{r}$, then leads to the interaction Hamiltonian, $H = -\mu_1\xi_1 - \mu_2\xi_2$. Fundamentally, a two-photon absorption process can then be charaterized by the time-averaged probability per molecule for the system to reside in the upper state $|u\rangle$; viz.,

$$\bar{P}_{u\ell} = \overline{|\langle u|\psi(\vec{r},t)\rangle|^2} \ , \tag{2}$$

where the over-bar denotes a time-average. An analytic form of the wave function is often obtained using a second-order perturbation solution[16] of Schrodinger's equation or the equivalent time-evolution operators.[30] By retaining only those terms selected by the near-resonance condition, $\omega_{u\ell} - \omega_1 - \omega_2 \to 0$ where $\omega_{u\ell}$ is the transition frequency, the steady-state result obtained is

$$\bar{P}_{u\ell} = \frac{\overline{|\xi(\vec{r},t)\xi^*(\vec{r},t)|^2}}{16\hbar^2[(\omega_{u\ell} - \omega_1 - \omega_2)^2 + \gamma_u^2]} \ |M_{u\ell}|^2 \ , \tag{3}$$

with the strength of the interaction determined by the molecular transition moments through the term

$$|M_{u\ell}|^2 = \left|\sum_m \left[\frac{\langle u|\mu_2|m\rangle\langle m|\mu_1|\ell\rangle}{\hbar(\omega_{m\ell} - \omega_1)} + \frac{\langle u|\mu_1|m\rangle\langle m|\mu_2|\ell\rangle}{\hbar(\omega_{m\ell} - \omega_2)}\right]\right|^2 . \tag{4}$$

Field polarization effects in Eq. (4) manifest themselves only in transitions where no change in angular momentum occurs. In the case of NO γ-band transitions, field polarization has no influence on the relative rotational line strengths of any branches because of

the difference in orbital angular momentum between initial and final electronic states.[28]

To obtain the semiclassical solutions represented by Eq. (3), a damping term characterized by the coefficient γ_u was added phenomenologically to the Schrodinger equation, leading to an important implication in the application of this theory to a real experiment. The fact that Eq. (3) results from a steady-state solution in which the field amplitudes are constant requires that the use of Eq. (3) be limited to experiments in which the laser pulse duration Δt_p is long compared with the dephasing time of the upper state, $1/\gamma_u$. An indicator of the dephasing time is the homogeneous spectral width $\Delta\omega_{u\ell}$, so that our treatment may be considered valid only for $\Delta t_p >> 2\Pi/\Delta\omega_{u\ell}$. As an example, for a typical laser pulse duration of 5 ns, Eq. (3) is roughly applicable only for conditions in which the transition homogeneous spectral width exceeds 0.01 cm^{-1}. Since collision-broadened line widths for NO γ-bands at 300 K are approximately 1 cm^{-1}/atm,[31,32] we can then expect validity only for pressures greater than ≈10 torr at 300 K.

A second important consideration in the use of Eq. (3) for an experimental analysis arises by noting that the time-averaged product of the instantaneous fields must be computed considering the field coherence.[33] Yet, experimentally, we know only the amplitudes $|\xi_1|^2$ and $|\xi_2|^2$. Glauber[34] introduced a second-order correlation

function to deal with the effect that can be written in an equivalent classical form as

$$G^{(2)} = \langle |\xi(\vec{r},t)\xi^*(\vec{r},t+\tau)|^2\rangle / \langle |\xi_1|^2\rangle \langle |\xi_2|^2\rangle \ . \qquad (5)$$

The angle-brackets now denote the use of a statistically defined and ensemble-averaged field with fluctuations described in terms of a prescribed coherence time. In general, for chaotic fields, $G^{(2)} = 2$. Examples include the field from a multimode laser with independently oscillating modes or the combined field from two uncorrelated laser sources. Conversely, for a single-mode laser, $G^{(2)} = 1$, and for a mode-locked laser, $G^{(2)}$ takes values equal in magnitude to the number of coupled modes. Furthermore, the correlation is altered when the absorption of a chaotic field is significant, causing $G^{(2)}$ to approach unity for the emerging beam.[35] To specifically isolate the experimentally dependent effects we therefore rewrite Eq. (3) in the form:

$$\bar{P}_{u\ell} = \frac{4\pi^3 |M_{u\ell}|^2}{\gamma_u \hbar^2 c^2 n_1 n_2} g(\omega_{u\ell} - \omega_1 - \omega_2) G^{(2)} I_1(\omega_1) I_2(\omega_2) \ , \qquad (6)$$

where n_1 and n_2 are the refractive indices at frequencies ω_1 and ω_2, respectively, and the field intensities have been defined according to $I_i(\omega_i) = (cn_i/8\pi)|\xi_i|^2$. We have also introduced the normalized line shape function $g(\omega_{u\ell} - \omega_1 - \omega_2)$ written as an example for homogeneously broadened transitions,

$$g(\omega_{u\ell} - \omega_1 - \omega_2) = \frac{1}{\pi} \frac{\gamma_u}{(\omega_{u\ell} - \omega_1 - \omega_2)^2 + \gamma_u^2} \ .$$

The significance of field coherence on two-photon absorption was demonstrated experimentally by Krasinski et al.[36] Their work illustrates that uncertainties due to the effect are conveniently avoided by accepting the tendency of most lasers to oscillate on multiple longitudinal modes. The resulting value of $G^{(2)} \cong 2$ then remains fixed when the absorption is weak and provides twice the absorption obtained with a correlated beam.

A two-photon absorption cross section can be defined by noting that in steady state the power loss and power gain for the molecular system are equal. To define each, the energy per unit volume deposited into state $|u\rangle$ is described by

$$E_u = \hbar\omega_{u\ell} N_\ell \bar{P}_{u\ell} \ , \tag{7}$$

where N_ℓ is the number density of state $|\ell\rangle$. Then, an expression for power gain that is dependent on a two-component field of intensity $I_1(\omega_1) + I_2(\omega_2)$ can be written as

$$\left(\frac{dE_u}{dt}\right)_{GAIN} = \sigma_{u\ell} N_\ell [I_1(\omega_1) + I_2(\omega_2)] \ , \tag{8}$$

thus defining the cross section, $\sigma_{u\ell}$. Equating Eq. (8) to the power loss due to damping given by

$$\left(\frac{dE_u}{dt}\right)_{LOSS} = \gamma_u E_u \ , \tag{9}$$

and incorporating Eqs. (6) and (7), a microscopic definition of the two-photon cross section is obtained as

$$\sigma_{u\ell} = \frac{\alpha_{u\ell}^{(2)}}{n_1 n_2} g(\omega_{u\ell} - \omega_1 - \omega_2) G^{(2)} \frac{I_1 I_2}{I_1 + I_2} , \qquad (10)$$

where the coefficient characterizing the absorbing medium for a specific transition is

$$\alpha_{u\ell}^{(2)} = \frac{4\pi^3 \hbar \omega_{u\ell}}{\hbar^2 c^2} |M_{u\ell}|^2 . \qquad (11)$$

Note that $\alpha_{u\ell}^{(2)}$ still retains some dependence on the field frequencies appearing in Eq. (4). However, within the conditions of this derivation where all intermediate states are assumed to be far from resonance (i.e., $\omega_{m\ell} - \omega_i >> \gamma_m$), the dependence of $|M_{u\ell}|^2$ on frequency over the range of the line-shape function $g(\omega_{u\ell} - \omega_1 - \omega_2)$ will be negligible. Thus, $\alpha_{u\ell}^{(2)}$ may be regarded as a two-photon transition strength that is independent of any experimental conditions. Using these results, we can now examine the macroscopic aspects of the absorption process in terms of the parameters of quantitative importance in a laboratory experiment.

B. Spectral Intensities

In this section, we emphasize the effects of comparable transition and laser spectral widths. The practical applications considered include bulk gas densities in which homogeneous collisional broadening is a substantial contributor to the transition spectral width. Then, the use of extremely narrow laser spectral widths provides only minor enhancements in the absorptive coupling to the

gas, and we may retreat to the simpler experimental arrangement in which laser spectral widths obtained without intracavity etalons are acceptable.

To formulate the total rate of energy absorption and to incorporate the spectral aspects of the incident field, we define the spectral intensity I_ω such that the field intensity in the frequency range ω to $\omega + d\omega$ at the spatial location z, is $I_\omega(z)d\omega$. Then, from the results of the previous section, a one-dimensional absorption process can be described on a laboratory scale for two specific frequency components by

$$\frac{\partial}{\partial z} I_{\omega_1}(z)d\omega_1 = -N_\ell(1 - \beta_{u\ell})\delta_{u\ell} I_{\omega_1} I_{\omega_2} d\omega_1 d\omega_2$$

and (12)

$$\frac{\partial}{\partial z} I_{\omega_2}(z)d\omega_2 = -N_\ell(1 - \beta_{u\ell})\delta_{u\ell} I_{\omega_2} I_{\omega_1} d\omega_2 d\omega_1 \ ,$$

where we define the parameters

$$\beta_{u\ell} = g_\ell N_u / g_u N_\ell \quad \text{and} \quad \delta_{u\ell} = \alpha^{(2)}_{u\ell} g(\omega_{u\ell} - \omega_1 - \omega_2) G^{(2)} \ ,$$

and denote the upper and lower state number densities and degeneracies as N_u, N_ℓ, and g_u, g_ℓ, respectively. Refractive indices have been set to unity. Equations (12) include the two-photon stimulated emission term $\beta_{u\ell}$, which is required to describe the effects of transition saturation. We shall show that saturation becomes a practical limitation to the maximum fluorescence signal obtainable and that it can be achieved with commercially available

lasers. We also recognize that the field intensities leading to saturation can exceed the limits for which two-photon absorption is the only significant energy dissipation mechanism in the interaction process. However, the treatment of saturation effects here is intended to indicate the onset of limiting processes rather than to describe them in detail.

Equations (12) can be integrated over a path length L to give

$$\frac{I_{\omega_1}(L)}{I_{\omega_1}(0)} = \frac{I_{\omega_1}(0)d\omega_1 - I_{\omega_2}(0)d\omega_2}{I_{\omega_1}(0)d\omega_1 - I_{\omega_2}(0)d\omega_2 \exp\{L\delta_{u\ell}N_\ell(1 - \beta_{u\ell})[I_{\omega_2}(0)d\omega_2 - I_{\omega_1}(0)d\omega_1]\}} , \tag{13}$$

and similarly for $I_{\omega_2}(L)$, but with ω_1 and ω_2 notation transposed. In this application, we are interested in propagation over minimum path lengths to obtain high spatial resolution. We can control the effective path length with focusing and the optical depth by reducing N_ℓ. As a consequence, we can generally create conditions in which the absorbing medium is optically thin such that

$$L\delta_{u\ell}N_\ell(1 - \beta_{u\ell})I_\omega(0)d\omega << 1$$

for both frequency components. Equation (13) then reduces to:

$$[I_{\omega_1}(0) - I_{\omega_1}(L)]d\omega_1 = L\delta_{u\ell}N_\ell(1 - \beta_{u\ell})I_{\omega_1}(0)I_{\omega_2}(0)d\omega_1 d\omega_2 , \tag{14}$$

and similarly for I_{ω_2}. In an irradiated area, A_o, the total rate of energy absorption, considering both frequency components, in an optically thin medium, is then

$$\frac{1}{A_o}\frac{d}{dt}E(\omega_1,\omega_2) = [I_{\omega_1}(0) - I_{\omega_1}(L)]d\omega_1 + [I_{\omega_2}(0) - I_{\omega_2}(L)]d\omega_2$$

$$= L\delta_{u\ell}N_\ell(1 - \beta_{u\ell})2I_{\omega_1}(0)I_{\omega_2}(0)d\omega_1 d\omega_2 \ . \qquad (15)$$

If we now consider the case in which each frequency component originates from one of two distinguishable laser sources, Eq. (15) can be used to compute the total rate of energy absorption at all frequencies in terms of the experimentally known power per unit area in each beam, P_L/A_o and P_L'/A_o, and the normalized line-shape functions for each beam, $g_L(\omega_L - \omega_1)$ and $g_L'(\omega_L' - \omega_2)$. The prime notation distinguishes one laser source and its parameters from the other. The spectral intensity in one beam becomes

$$I_\omega(0)d\omega = \frac{P_L}{A_o}g(\omega_L - \omega)d\omega \ ,$$

where ω_L is the laser center-frequency. Integrating Eq. (15) over all frequencies, the total rate of energy absorption per unit area is then

$$\frac{1}{A_o}\frac{dE_T}{dt} = L\alpha_{u\ell}^{(2)}G^{(2)}N_\ell(1 - \beta_{u\ell})\frac{P_L P_L'}{A_o^2}\bar{g} \ , \qquad (16)$$

where

$$\bar{g} = \frac{1}{2}\int_0^\infty\int_0^\infty 2g(\omega_{u\ell} - \omega_1 - \omega_2)g_L(\omega_L - \omega_1)g_L'(\omega_L' - \omega_2)d\omega_1 d\omega_2 \ .$$

The factor of 2 in the integrand comes from Eq. (15). However, the range of the integrals has been written to contain each of the functions g_L and g_L' twice. Hence, the factor of 1/2 is also required. An analytically convenient form of $\bar{g}$ is finally given by

$$\bar{g} = \int_{-\infty}^{\infty} \int_{-\infty}^{\infty} g(\omega_{u\ell} - \omega_1 - \omega_2) g_L(\omega_L - \omega_1) g_L'(\omega_L' - \omega_2) d(\omega_L - \omega_1) d(\omega_L' - \omega_2) \ . \tag{17}$$

The same formulation is obtained when both frequency components are contained in a single laser source. In that case, the primed and unprimed terms are identical.

C. Line-Shape Integrals

Analytic solutions to the line-shape integral $\bar{g}$ can be obtained for several interesting cases. The simplest is the case most frequently considered in the literature,[13] in which the transition spectral width is very large compared with that of either laser beam. The normalized line-shape functions of both laser beams may then be approximated by Dirac delta functions and

$$\bar{g} \cong g(\omega_{u\ell} - \omega_L - \omega_L') \ . \tag{18}$$

When the finite spectral widths of the laser must be considered, an analytic solution is possible for Gaussian line-shape functions of the form

$$g(\omega_o - \omega) = \frac{(4\ln 2/\pi)^{1/2}}{\Delta\omega} \exp\left[-4\ln 2 \left(\frac{\omega_o - \omega}{\Delta\omega}\right)^2\right], \tag{19}$$

where $\Delta\omega$ is the full width at half-maximum. Integration of Eq. (17) then leads to

$$\bar{g} = \left[\frac{4\ln 2/\Pi}{\Delta\omega_{u\ell}^2 + \Delta\omega_L^2 + \Delta\omega_L'^2}\right]^{1/2} \exp\left[-4\ln 2\,\frac{(\omega_{u\ell} - \omega_L - \omega_L')^2}{\Delta\omega_{u\ell}^2 + \Delta\omega_L^2 + \Delta\omega_L'^2}\right], \quad (20)$$

where no distinction is necessary regarding beams from separate sources or from the same source beyond that implied by the notation. In the latter case, primed and unprimed variables again become identical. Note from Eq. (20) that, as expected, maximum absorptive coupling occurs when both incident beams are at resonance (i.e., $\omega_{u\ell} - \omega_L - \omega_L' = 0$) and their spectral widths are minimized. However, once the laser spectral widths are less than half of the transition width ($\Delta\omega_L < \Delta\omega_{u\ell}/2$), more than 0.8 of the maximum possible coupling has been achieved. If signal-to-noise ratio is the significant parameter to maximize, then only the root of that value (0.9) is important, and efforts to further reduce the laser spectral widths will yield a small return.

D. Molecular Dynamics

The previous results are now applied to analyze the nonequilibrium response of the two-photon-absorbing medium to a laser pulse. As stated previously, the laser pulse is assumed to be long compared with the collisional dephasing time, $2\Pi/\Delta\omega_{u\ell}$, thereby justifying the use of a rate-equation description. On the other hand, the laser pulse is considered to be short compared with the fluorescene decay times including quenching. We can then neglect the presence of

upper state decay during excitation and decouple the excitation and decay processes. This condition is justified for excitation of the NO γ-band system at all low-density conditions in which the absolute absorptivity is usually measured and for most wind-tunnel conditions, by noting that the effective fluorescence lifetimes of NO with N_2 as a quenching partner[10,37] – for N_2 at 0.1 amagat ($2.5 \times 10^{18}/cm^3$) – is 70 ns, and the laser pulse widths are typically 5 ns. However, cases for higher density or more efficient quenching partners could require the opposite assumption in the extreme where the excitation and decay processes maintain a steady-state equilibrium with one another. This latter sitatuion is more difficult to treat precisely because the paths for rotational energy redistribution among the upper and lower vibronic states and their associated rates must be described in detail.[38,39] The difference in the two extreme cases has an effect on the signal-to-noise ratios predicted, but not on the temperature indicated. Since the latter case is impractical to analyze when the objective is to measure an absolute two-photon absorptivity, such measurements would not be made at those conditions. Thus, we choose the former case as the only one of importance for a quantitative analysis in this application.

With the foregoing assumption, only the specific upper and lower states selected by resonant absorption are coupled during the laser pulse. Their populations are related to the energy absorption rate given by Eq. (16) according to

$$\hbar\omega_{u\ell}\frac{dN_\ell}{dt} = -\frac{1}{A_o L}\frac{dE_T}{dt} , \tag{21}$$

$$\frac{dN_u}{dt} = -\frac{dN_\ell}{dt} , \tag{22}$$

and

$$N_u + N_\ell = N_\ell^\circ(1 + e^{-\hbar\omega_{u\ell}/kT}) , \tag{23}$$

where N_ℓ° is the initial lower-state population number density. If we restrict our interest only to temperatures where $\hbar\omega_{u\ell}/kT >> 1$ (note: $\hbar\omega_{u\ell}/k \approx 64000$ K for NO γ-bands), and define the parameters

$$Q_L = \bar{g}\frac{G^{(2)}}{A_o^2}\int_0^\infty P_L(t)P_L'(t)dt , \tag{24}$$

$$Q_{u\ell} = \hbar\omega_{u\ell}/\alpha_{u\ell}^{(2)} , \tag{25}$$

we may integrate Eqs. (21) and (22) using Eq. (16). The result gives the nonequilibrium population densities remaining after the laser pulse and before the onset of decay as

$$N_\ell/N_\ell^\circ = \frac{g_\ell/g_u + e^{-(1 + g_\ell/g_u)Q_L/Q_{u\ell}}}{1 + g_\ell/g_u} , \tag{26}$$

$$N_u/N_\ell^\circ = \frac{1 - e^{-(1 + g_\ell/g_u)Q_L/Q_{u\ell}}}{1 + g_\ell/g_u} . \tag{27}$$

E. Fluorescence Energy and the Signal-to-Noise Ratio

Knowing the population densities, the subsequent fluorescence energy E_f from the entire electronic band can be related to the

experimental parameters Q_L and $Q_{u\ell}$. To do that, we define a time-dependent fluorescence power per unit volume, $P_f(t)$, emitted into 4Π steradians from the volume A_oL such that

$$E_f = A_oL \int_0^\infty P_f(t)dt \ . \tag{28}$$

The fluorescence power summed over all transitions originating from the upper electronic state can be written

$$P_f(t) = N_u(t) \sum_{u'\ell'} A_{u'\ell'}\hbar\omega_{u'\ell'}N_{u'}/N_u \ , \tag{29}$$

where $A_{u'\ell'}$ is the Einstein coefficient for spontaneous emission. The summation includes dipole-allowed transitions to all lower states and accounts for the thermalization of rotational and vibrational energy in the upper electronic state during the decay period. It does not include self-absorption and radiative trapping, which, in the case of NO $\gamma(0,0)$ band excitation at ambient temperature, could reduce the fluorescence power by a maximum of about 25%, based on the Franck-Condon factors for the γ-band.[40] Experimentally, the summation in Eq. (29) may be evaluated by defining a mean transition energy, $\hbar\omega_o$, and measuring and <u>electronic state</u> fluorescent lifetime τ_f such that in the absence of quenching

$$\sum_{u'\ell'} A_{u'\ell'}\hbar\omega_{u'\ell'}N_{u'}/N_u \equiv \hbar\omega_o/\tau_f \ . \tag{30}$$

The assumption implicit in Eq. (30) is that the lifetimes of individual rotational states are equal. When quenching is included,

the effective lifetime, τ_u, is composed of τ_f and a collisional component, τ_c, also known experimentally.[10,37] The three are related by

$$1/\tau_u = 1/\tau_f + 1/\tau_c \ . \tag{31}$$

The upper state population then decays according to

$$N_u(t) = N_u(0)e^{-t/\tau_u} \ , \tag{32}$$

and the combination of Eqs. (27)-(32) leads to the result,

$$E_f = A_o L N_\ell^\circ \frac{\hbar\omega_o}{1 + \tau_f/\tau_c}\left[\frac{1 - e^{-(1 + g_\ell/g_u)Q_L/Q_{u\ell}}}{1 + g_\ell/g_u}\right]. \tag{33}$$

The effects of saturation are contained in the bracketed term in Eq. (33). The two-photon absorptivity parameter, $\alpha_{u\ell}^{(2)}$, may be conveniently evaluated in a laser-induced fluorescence experiment by operating at laser powers in the linear range where $(1 + g_\ell/g_u)Q_L/Q_{u\ell} << 1$. Then, in terms of experimental parameters,

$$\alpha_{u\ell}^{(2)} \cong (1 + \tau_f/\tau_c)\frac{E_f/Q_L}{A_o L N_\ell^\circ} \ . \tag{34}$$

Finally, the signal-to-noise ratio S/N, for signals limited by photon-statistical noise, is $(\bar{n})^{1/2}$, where $\bar{n}$ is the number of photons detected during the measurement period. In the notation of Eq. (33)

$$S/N = (\phi\eta E_f/\hbar\omega_o)^{1/2} \ , \tag{35}$$

where ϕ is the efficiency of the collection optics and η is the quantum efficiency of the photodetector.

F. Focusing Effects

Since the two-photon absorption process has no explicit dependence on phase correlation, the effects of focusing may be treated simply in terms of spatial variations in the field intensity. For example, if $I(z,r)$ is the local field intensity of an axisymmetric beam, the average power per unit area at any axial location may be written as

$$\frac{P_L}{A} = \frac{2\pi}{A(z)} \int_0^\infty I(z,r) r \, dr \ , \tag{36}$$

where $A(z)$ is a characteristic cross section for a given radial profile. Assuming that both beams in the two-photon process have the same focusing parameters, the steps leading to Eq. (24) can then be repeated using Eq. (36) in place of P_L/A_o. The only change is a modification to Eq. (24) in which the laser power parameter is redefined to include the focusing integral Φ_L according to

$$Q_L = \Phi_L \frac{\bar{g} G^{(2)}}{A_o^2} \int_0^\infty P_L(t) P_L'(t) dt \ . \tag{37}$$

Here, A_o becomes the minimum area at the focal point ($z = 0$). The focusing integral has the general form for two-photon processes of

$$\Phi_L = \frac{A_o}{L} \int_{-L/2}^{L/2} \frac{dz}{A(z)} \ , \tag{38}$$

where L is the axial length over which fluorescence emission is observed. A simple example is obtained by choosing a diffraction-limited Gaussian beam profile where the axial variation through a

focal region is given by $A(z) = A_o[1 + (z/b)^2]$. The confocal parameter is then $b = A_o/\lambda$ for wavelength, λ, and Eq. (37) yields

$$\Phi_L = \frac{\arctan(L/2b)}{L/2b} \quad . \tag{39}$$

Note that $\Phi_L \to 1$ in the long focus limit ($L/2b \to 0$) as required and, thus, is independent of the confocal parameter. However, in Eq. (33), E_f remains dependent on A_o, thus requiring A_o to be known if $\alpha_{u\ell}^{(2)}$ is to be measured. Conversely, in the short focus limit ($L/2b \to \infty$), $\Phi_L \to \Pi A_o/L$, and E_f becomes independent of A_o in the linear range of Eq. (33). Since A_o is generally difficult to measure accurately, the short focusing limit becomes a desirable region for minimizing experimental errors when the objective is to measure the absolute two-photon absorptivity.

IV. Applications

We have argued that the foregoing analysis in which the excitation and delay processes are decoupled is applicable to conditions where the fluorescence decay times are long compared with the laser pulse width. Two applications meeting that criterion for a laser pulse duration of 5 ns are the measurement of two-photon absorptivity in a low-pressure, nonflowing cell and the measurement of fluctuating temperatures in typical supersonic turbulent flows. In this section, we analyze first the nonflowing cell condition where we have made a preliminary measurement of the two-photon absorptivity in NO. That result is then used to predict the signal-to-noise ratios (S/N)

obtainable in a supersonic wind-tunnel environment of general interest. Finally, the sensitivity of the technique for measuring temperature is evaluated and used to guide the choice of the most advantageous spectral features in the NO γ-band.

A. Preliminary Absorptivity Measurements

The absolute two-photon absorptivity for the $NO(A^2\Sigma^+, v' = 0 \leftarrow X^2\Pi_{1/2}, v'' = 0)$, $S_{11} + R_{21}(J'' = 7\text{-}1/2)$ transition was measured in a nonflowing cell containing 1.0 torr of NO at room temperature. The S_{11} and R_{21} branches are satellites separated in energy only by the spin-splitting of their upper states, which is smaller than the Doppler width. As Fig. 1 indicates, the $J'' = 7\text{-}1/2$ line has the greatest absorptivity in the vibronic band; Fig. 5 shows that it can be spectrally isolated for line widths less than 0.5 cm^{-1}. Given the absorptivity for one line, the absorptivity of all other rotational transitions in the same vibronic band can be evaluated using the line intensity factors determined theoretically for intermediate Hunds coupling by Halpern et al.[28] We have found that a synthetic spectrum predicted using Halpern's theory agrees very well with the relative line intensities obtained experimentally.

The measurement was made using a Molectron DL200 tunable dye laser pumped by a 400-kW N_2 electric-discharge laser. The 5 ns Gaussian-like temporal waveform was spatially filtered to provide a fairly homogeneous beam with a pulse energy of 5-10 μJ. An

average spectral width of 0.1 cm^{-1} was achieved, while retaining ease in tunability, by operating the grating in seventh order without an intracavity etalon. The broad-band fluorescence was collected with f/1 quartz optics and imaged through an aperture that limited observation to a 0.5-mm path length along the laser beam axis through its focal region. Fluorescence intensity was detected with a solar-blind photomultiplier system having a response time of 15 ns and a low-pass absorption filter. The signal, with a decay time of approximately 150 ns, was integrated and averaged using a box-car integrator. The integrated output was recorded as the laser was tuned through the line peak, while a second channel monitored the long-term variations in average laser power. The collection optics were calibrated radiometrically by filling the cell with various gases up to 1 atm and recording the Rayleigh scattering signal at 266 nm from the fourth harmonic of an Nd-YAG laser. The calibration included a correction for the spectral response of the detector system over the range of the NO fluorescence spectrum. The diameter of the laser beam and, hence, its intensity distribution in the focal region, was estimated by assuming an axisymmetric Gaussian profile and focusing through calibrated apertures to find the diameter that transmitted 80% of the beam energy. However, the laser spatial profile was not entirely homogeneous, making its intensity distribution one of the most uncertain experimental variables. Other uncertainties include the method of evaluating the average

laser power integral, Q_L [Eq. (37)], and the measurement of laser and transition spectral widths. Although we believe that the combined effects of all uncertainties contribute less than a factor of 10 to the absorptivity measured, they can be reduced significantly with an improved data acquisition method and a laser source having greater pulse energy and spectral control. For those reasons, we regard our measurement as preliminary, although we consider it to be sufficiently accurate for the evaluation of S/N capabilities in this study.

An absorptivity, $\alpha_{u\ell}^{(2)} = 6 \times 10^{-20}$ cm^4/J, was obtained for the $S_{11} + R_{21}$ (J" = 7-1/2) transition using Eq. (34) and assuming quenching rates equal to those measured under similar conditions.[10,37] The measurement was found to be properly dependent on the average laser power and cell pressure. The corresponding matrix element parameter defined by Eq. (4) is then $|M_{u\ell}|^2 = 6 \times 10^{-52}$ cm^6. This value may be compared with the measurement of Hochstrasser et al.[22] who used a greatly different experimental approach (with its own sources of uncertainty) and who report the only other related measurement in NO known to us. They studied the O_{12} (J" = 6-1/2) transition and obtained a value of $|M_{u\ell}|^2 = 0.3 \times 10^{-51}$ cm^6. Using the appropriate ratio of line intensity factors,[28] our measurement implies a value of $|M_{u\ell}|^2 = 3 \times 10^{-51}$ cm^6 for the O_{12} (J" = 6-1/2) transition. Thus, we are somewhat assured that the absorptivity values to be used here are within a reasonable range of the correct

value. If the error is a factor of 10, predictions of S/N will be in error by $(10)^{1/2}$ and any conclusions regarding the feasibility of using two-photon excitation to measure temperature will be unaffected.

B. Signal-to-Noise Ratios at Supersonic Wind-Tunnel Conditions

An area of significant interest in modern fluid mechanics is the characterization of turbulent flows at transonic and low supersonic speeds. Nonintrusive measurement of fluctuations in the variables of state, including temperature, guide the modeling of such flows. Typically, test conditions involve temperatures below 300 K and densities in the range of 0.1 amagat. Measurements that can be made in volumes with the largest dimension less than 1 mm are of greatest interest. Fluctuation amplitudes can be expected to remain less than 10% of the mean value, thereby requiring measurements with S/N substantially greater than 10. Here, we estimate the S/N limited by photon-statistical noise [Eq. (35)] at typical wind-tunnel conditions listed in Table I. We have limited the NO concentration to 250 ppm to reduce the hazards of toxic gas mixtures in large-volume wind tunnels and to minimize the loss of signal due to radiative trapping. We have chosen N_2, rather than air, as the bulk gas to minimize the effects of quenching and the loss of NO through oxidation.

The resulting S/N values are shown in Fig. 6 for two focal diameters in the long-focus regime. Electric breakdown limits are

based on an estimated breakdown intensity of 3.5×10^{10} W/cm^2 at these conditions.[41] The breakdown limit serves only to indicate the onset of strong field effects not included in this analysis. It warns that strong field and saturation effects all become important at about the same power densities. Also included in Fig. 6 is the S/N for spontaneous rotational Raman excitation of N_2 based on a cross section of 5×10^{-30} cm^2/sr and the favorable but impractical assumption that the Raman scattering in a single rotational line can be spectrally isolated using optical elements with 10% transmission.

The practicality of using two-photon fluorescence excitation to probe individual rotational transitions becomes evident when we note that several commercially available tunable dye lasers can exceed 10 mJ of pulse energy at 450 nm. Thus, the levels of S/N limited by saturation should be attainable with the experimental configuration shown in Fig. 4. Since the same saturation limits occur in single-photon excitation, the higher pulse energies required for two-photon excitation do not impose a penalty in practice. In fact, the greater difficulty in separating scattered laser light at single-photon wavelengths from the fluorescence signal will, most likely, lead to collection optics with much lower efficiency and, hence, lower S/N, even at saturation. As expected, Raman scattering, even in a highly idealized form, is not a feasible alternative for measuring fluctuating temperatures. At laser energies giving S/N > 1, electric breakdown obviates the measurement. Finally, we

note that the uncertainties in two-photon absorptivity cause a related uncertainty in the horizontal (energy scale) position of the curves in Fig. 6. However, since the uncertainty is believed to be less than a factor of $(10)^{1/2}$, it will have no effect on the qualitative conclusions drawn here.

The vertical positions of the curves in Fig. 6 including the saturation levels depend on the quenching ratio, τ_f/τ_c. Zacharias et al.[10] and Asscher and Haas[37] report measured quenching rates for NO γ-band fluorescence at room temperature for a range of pressures. If we make the rough approximation that quenching rate varies with density and temperature as does the collision frequency, then we can summarize the results of Zacharias et al. and Asscher and Haas for any experimental condition by

$$\tau_f/\tau_c = C \frac{\sigma_x}{\sigma_{NO}} N_x T^{1/2} , \qquad (40)$$

where σ_x/σ_{NO} is the ratio of quenching cross section for species X to that for self-quenching of NO, N_x is the number of density of species X, and T is the kinetic temperature. The temperature dependence in Eq. (40) derives from hard-sphere interactions and is very approximate. For N_x in units of cm^{-3} and T in °K, the proportionality constant in Eq. (40) is $C = 2.5 \times 10^{-18}$. From Asscher and Haas,[37] we obtain $\sigma_{N_2}/\sigma_{NO} = 0.02$, $\sigma_{O_2}/\sigma_{NO} = 0.76$, and estimate $\sigma_{AIR}/\sigma_{NO} = 0.17$; all for NO γ-band fluorescence quenching. From these values and from Eqs. (33) and (35), the S/N for air at

the same conditions would equal 40% of the S/N shown for N_2 quenching, thus, still giving reasonable values at available laser pulse energies. However, the application of this technique at significantly higher densities or temperatures or both, such as in a combustion process, will render it less favorable as quenching diminishes the fluorescence signal. Hence, we conclude that even though saturated signals may be achieved with two-photon excitation of NO, the signal-to-noise ratios are large enough for fluctuating temperature measurements only at temperatures and densities below ambient values for most quenching environments. Nevertheless, conditions meeting those criteria are directly opposite to those in which successful Raman techniques have been applied, thus exemplifying the unique features of two-photon fluorescence excitation.

C. Temperature Sensitivity and the Selection of Spectral Features

As the two-photon spectra in Figs. 1 and 5 show, line intensities in a given rotational branch are strongly dependent on the initial state rotational quantum number, J". If we are to use the ratio of fluorescence energy from the excitation of two initial states to determine the temperature, as Eq. (1) suggests, then we must either input more laser energy into the weaker transition or note that the S/N for determining temperature, that is, the temperature sensitivity, will not be the same as the S/N given in Fig. 6 for detecting fluorescence from a single transition. In this section, we consider the later case by assuming that both transitions receive equal excitation energy and we determine the temperature measurement sensitivity.

The results will then guide our choice of initial state transition pairs for a given experimental condition.

To quantify the results, we note that the fluorescence energy $E_f(J'')$ due to absorption by an initial rotational state, J'', follows the proportionality

$$E_f(J'') \sim N^\circ_{J''} \frac{\mathcal{S}_{J'J''}}{2J'' + 1} ,$$

where $N^\circ_{J''}$ is the initial rotational state population and $\mathcal{S}_{J'J''}$ is the rotational line intensity factor. Halpern et al.[28] show that, except for very low values of J'', the factor $\mathcal{S}_{J'J''}/(2J'' + 1)$ is only a weak function of J'', especially for the intense $S_{11} + R_{21}$ branch. Thus, for the purposes of this discussion, we may assume that the variation of line intensity with J'' shown in Fig. 5 for a given rotational branch is dominated by variations in $N^\circ_{J''}$. Then, in general, the ratio of fluorescence energies for transitions in the same branch will vary with temperature according to the Boltzmann relation,

$$\frac{E_f(J_1)}{E_f(J_2)} \cong \frac{(2J_1 + 1)}{(2J_2 + 1)} e^{-\frac{\theta_r}{T}[J_1(J_1 + 1) - J_2(J_2 + 1)]} , \qquad (41)$$

where $\theta_r \equiv \hbar B_e/k$ is the characteristic rotational temperature for the molecular rotor, and J_1, J_2 denote the initial-state rotational quantum numbers of two transitions. If we now introduce a noise component, ε_J, onto the signal so that $E_f(J) \sim N_J(1 \pm \varepsilon_J)$, we can compute the corresponding noise component on temperature $\eta_{J_1J_2}$

such that its perturbed value is $T(1 \pm \eta_{J_1J_2})$. Equation (41) then leads to

$$(1 + \eta_{J_1J_2})^{-1} = \frac{\ln\left(\frac{1 + \varepsilon_{J_1}}{1 - \varepsilon_{J_2}}\right)}{\frac{\theta_r}{T}\left[J_2(J_2 + 1) - J_1(J_1 + 1)\right]}, \qquad (42)$$

where $\eta^{-1}_{J_1J_2}$ can be regarded as the temperature-S/N for the line-pair and $\varepsilon^{-1}_{J_1}, \varepsilon^{-1}_{J_2}$ are the fluorescence-S/N of each line.

If the noise is again considered dominated by photon-statistical noise, then $\varepsilon^{-1}_{J_1} = K[E_f(J_1)]^{1/2}$ where K is a constant. We may now compute the values of $\eta_{J_1J_2}$ for selected T, J_1, and J_2 by assigning a fluorescence-S/N to the more intense transition and relating ε_{J_1} and ε_{J_2} through Eq. (41). Note that if $\varepsilon^{-1}_{J_1} >> 1$ (large fluorescence-S/N), the resulting $\eta_{J_1J_2}$ is insensitive to the numerical value of ε_{J_1} used for the calculation, making our choice inconsequential. Some results are shown in Fig. 7 for $\varepsilon^{-1}_{J_1} = 100$ for cases (J_1 = 4-1/2, T = 100 K) and (J_1 = 7-1/2, T = 300 K). The two values of J_1 selected represent the most populated states of $NO(X^2\Pi, v'' = 0)$ at each temperature. Thus, larger J_1 values would result in lower temperature-S/N for all J_2. As the figure shows, temperature-S/N values up to 80% of the fluorescence-S/N for the more intense transitions are attainable with the proper choice of a J_1, J_2 pair. For example, at T = 300 K, the $S_{11} + R_{21}$ (J'' = 7-1/2) transition is the most intense making

$S_{11} + R_{21}$ ($J'' = 20\text{-}1/2$) the optimum partner for the pair. Figure 5 shows that both lines are well isolated for spectral widths less than 0.5 cm^{-1}. Similarly, at lower temperatures, $J'' = 4\text{-}1/2$ and $12\text{-}1/2$ become a more sensitive pair. Isolation of the $S_{11} + R_{21}$ ($J'' = 4\text{-}1/2$) line will require spectral widths less than 0.2 cm^{-1} but transitions for all $J'' \geq 12\text{-}1/2$ are well dispersed. Finally, note that since the $S_{11} + R_{21}$ branch is the most intense and transitions from an adequate range of initial states can be spectrally isolated, there is no advantage in using transitions from other branches or from two different branches.

VI. Summary

We have described and analyzed a laser-induced fluorescence technique that is especially suitable for measuring fluctuating temperatures in cold turbulent flows containing very low concentrations of nitric oxide. The method has been shown to be capable of resolving temperatures below 300 K with signal-to-noise ratios greater than 50:1 and with spatial resolution to volumes having submillimeter dimensions. This capability is unique and outside the range of all other nonintrusive techniques known to us for making similar measurements. The method relies on the two-photon excitation of selected ro-vibronic transitions in the $NO(A^2\Sigma^+, v' = 0 \leftarrow X^2\Pi, v'' = 0)$ γ-band spectrum. It is based on the use of commercially available lasers operating with high peak power

at visible wavelengths and with spectral bandwidths less than 0.5 cm^{-1}. Detection of the subsequent broad-band ultraviolet fluorescence is assumed to be obscured only by photon-statistical noise and limited by collisional quenching. Fluorescence quenching is shown not to obviate the measurement for most conditions of interest in supersonic turbulent flow research, but it becomes troublesome at densities greater than ambient. The maximum signal-to-noise ratios attainable are limited by transition saturation, rather than available laser pulse energy, making excitation using two-photon absorption equivalent in sensitivity to that attainable with single-photon absorption. Subsequent limits are imposed by strong field effects such as electric breakdown. The principal advantages of two-photon excitation are (1) the relative simplicity of tunable lasers at visible wavelengths, (2) the ease and enhanced efficiency in spectrally isolating molecular fluorescence from scattered laser light, and (3) the increased dispersion of some rotational branches in the two-photon spectrum. In particular, the latter feature gives the two-photon technique apparent greater utility for a wider range of bulk gas densities than its single-photon counterpart because individual collision-broadened transitions remain spectrally isolated at the highest densities.

This study also includes a unified analysis of the two-photon fluorescence excitation processes with a view toward establishing the experimental parameters of qualitative importance. The results

are applied to a preliminary laboratory determination of the two-photon absorptivity for a single NO γ-band rotational transition. The measurement is related to the only known literature value and found to agree within a factor of 10, in spite of significantly different measurement techniques. The measured absorptivity allows estimates to be made, with reasonable confidence, of the signal-to-noise ratios attainable for measuring temperature at a variety of experimental conditions. It also permits establishment of the range of conditions for which the technique is applicable and leads to a clear identification of the most sensitive spectral features for measuring temperatures.

Appendix: The Equivalence of Some Two-Photon Absorptivity Parameters

In an early review of two-photon absorption, Peticolas[3] described the cross section $\sigma_{u\ell}$ in terms of the incident laser photon flux F (photon cm^{-2} sec^{-1}). His result is analogous to Eq. (10). He then defined the absorptivity parameter

$$\delta = \sigma_{u\ell}/F \tag{43}$$

and equated the fractional absorption of light of intensity I according to

$$\frac{dI}{I} = \delta FNL \ , \tag{44}$$

where N is the number density of the absorbers and L is the path length. The parameter δ has since been used widely as a measure

of two-photon absorptivity, but primarily and most correctly for spectral systems in which the transition spectral width is very much greater than the laser spectral width. However, in this application where the spectral widths are comparable, its use becomes less precise. In this appendix, we show the equivalence of δ to our notation and then use the result to interpret the notation of Hochstrasser et al.[22] Comparison of our absorptivity measurement with that by Hochstrasser is then done without confusion regarding numerical constants.

To develop the equivalence, we start with an alternative form of Eq. (44) analogous to Eq. (12), viz.,

$$\frac{dF}{dz} = -\delta N_{\ell} F^2 \ , \tag{45}$$

where F is the total photon flux in a single-beam experiment. The associated spectral intensity can be written

$$I_{\omega} d\omega = \hbar\omega_L g(\omega_L - \omega) F d\omega \ , \tag{46}$$

where ω_L is the laser center-frequency and $g(\omega_L - \omega)$ is its line-shape function. Then, by combining Eqs. (45) and (46) and comparing with Eq. (12), with $\beta_{u\ell}$ neglected, we obtain

$$\delta = \delta_{u\ell} \hbar\omega_L g(\omega_L - \omega) d\omega \ . \tag{47}$$

Note that in the limit where the laser spectral width is very small, compared with the transition width, we may write $\delta \cong \delta_{u\ell} \hbar\omega_L$ and our formulation is essentially identical to that of Peticolas.[13] However, for other than the limiting case, the importance of defining

the spectral width associated with the photon flux is apparent from Eq. (47) and from the discussion leading to Eq. (20).

Equation (47) can be combined with Eq. (11) to obtain a definition of δ in terms of the dipole matrix element term, $|M_{u\ell}|^2$. Again, for the case in which the laser spectral width is very small,

$$\delta \cong \frac{8\pi^3}{c^2} \omega_L^2 g(\omega_{u\ell} - 2\omega) |M_{u\ell}|^2 G^{(2)} \quad . \tag{48}$$

If we compare Eq. (48) with a similar relation given by Hochstrasser et al.[22] and assume that their normalizing procedure gives a result independent of the coherence term, $G^{(2)}$, then their matrix element notation, $|\alpha^T_{xx}|^2$, is identical to our $|M_{u\ell}|^2$ with no extraneous constants and the numerical values of each may be compared directly.

The authors are grateful for the assistance of Dr. J. O. Arnold and for the calculations he made to evaluate the effects of fluorescence self-absorption on the absorptivity measurement. One of us (KPG) acknowledges support through NASA Contract NAS2-10351.

References

1. R. Goulard, "Optical Measurements of Thermodynamic Properties in Flow Fields, A Review," Paper 13, AGARD Conference Proceedings No. 193 on Applications of Non-Intrusive Instrumentation in Fluid Flow Research, AGARD-CP-193, May 1976.
2. S. A. Self and C. H. Kruger, J. Energy 1, 25 (1977).
3. C. W. Peterson, AIAA J. 17, 1352 (1979).
4. J. A. Smith and J. F. Driscoll, "The Electron Beam Fluorescence Technique Applied to Hypersonic Turbulent Flows," Paper 16, AGARD Conference Proceedings No. 193 on Applications of Non-Intrusive Instrumentation in Fluid Flow Research, AGARD-CP-193, May 1976.
5. S. Lederman, Prog. Energy Combust. Sci. 3, 1 (1977).
6. R. J. Hall and A. C. Eckbreth, in "Laser Spectroscopy," Proc. Soc. Photo-Optical Inst. Eng. 158, 59 (1978).
7. D. R. Crosley and G. P. Smith, App. Optics 19, 517 (1980).
8. R. Goulard, in Laser Raman Gas Diagnostics, edited by M. Lapp and C. M. Penny (Plenum Press, 1974), p. 3.
9. G. F. Nutt, S. C. Haydon, and A. I. McIntosh, Chem. Phys. Lett. 62, 402 (1979).
10. H. Zacharias, J. B. Halpern, and K. H. Welge, Chem. Phys. Lett. 43, 41 (1976).
11. R. L. McKenzie, J. Chem. Phys. 66, 1457 (1977).
12. P. C. Jain, J. Phys. D: Appl. Phys. 13, 25 (1980).

13. W. L. Peticolas, Am. Rev. Phys. Chem. 18, 233 (1967).

14. A. Gold, in Quantum Optics, Proc. Int. Sch. Phys., E. Fermi Course 42, edited by R. Glauber (Academic Press 1969), p. 397.

15. J. M. Worlock, in Laser Handbook, Vol. 2, edited by T. Arecchi, F. Schulz-DuBois (North-Holland Pub. Co. 1972), p. 1323.

16. H. Mahr, in Quantum Electronics, A. Treatise, Vol. 1A, edited by H. Rabin, C. Tang (Academic Press 1975), p. 286.

17. N. Bloembergen and M. D. Levenson, in High-Resolution Laser Spectroscopy, edited by K. Shimoda (Springer-Verlag 1976), p. 315.

18. V. S. Letokhov and V. P. Chebotayev, Nonlinear Laser Spectroscopy (Springer-Verlag 1977).

19. R. Salomaa and S. Stenholm, J. Phys. B: Atom. Molec. Phys. 8, 1795 (1975).

20. R. Salomaa and S. Stenholm, J. Phys. B: Atom. Molec. Phys. 9, 1221 (1976).

21. R. Salomaa, J. Phys. B: Atom. Molec. Phys. 10, 3005 (1977).

22. R. M. Hochstrasser, G. R. Meredith, and H. P. Trommsdorff, Chem. Phys. Lett. 53, 423 (1978).

23. R. G. Bray, R. M. Hochstrasser, and J. E. Wessel, Chem. Phys. Lett. 27, 167 (1974).

24. J. A. Gelbwachs, P. F. Jones, and J. E. Wessel, Appl. Phys. Lett. 27, 551 (1975).

25. P. A. Freedman, Can. J. Phys. 55, 1387 (1977).

26. R. Wallenstein and H. Zacharias, Opt. Comm. 25, 363 (1978).

27. M. Asscher and Y. Haas, Chem. Phys. Lett. 59, 231 (1978).

28. J. B. Halpern, H. Zacharias, and R. Wallenstein, J. Mole. Spectrosc. 79, 1 (1980).

29. D. R. Grieser and G. H. Barnes, Appl. Opt. 19, 741 (1980).

30. A. Yariv, IEEE, J. Quant. Elec. QE-13, 943 (1977).

31. L. G. Dodge, J. Dusek, and M. F. Zabielski, "Line Broadening and Oscillator Strength Measurements for the Nitric Oxide $\gamma(0,0)$ Band," J. Quant. Spectrosc. Radiat. Transfer (to be published).

32. A. G. Gaydon and A. R. Fairbairn, Proc. Phys. Soc., London A67, 474 (1954).

33. R. Loudon, The Quantum Theory of Light (Oxford University Press, 1973).

34. R. J. Glauber, Phys. Rev. 131, 2766 (1963).

35. H. P. Weber, IEEE, J. Quant. Elect. QE-7, 189 (1971).

36. J. Krasinski, S. Chudzynski, W. Majewski, and M. Glodz, Opt. Comm. 12, 304 (1974).

37. M. Asscher and Y. Haas, J. Chem. Phys. 71, 2724 (1979).

38. R. P. Lucht and N. M. Laurendeau, Appl. Opt. 18, 856 (1979).

39. J. O. Berg and W. L. Shackleford, Appl. Opt. 18, 2093 (1979).

40. S. N. Suchard (ed.), Spectroscopic Data, Vol. 1B (Plenum, 1975).

41. R. G. Tomlinson, E. K. Damon, and H. T. Buscher, in Physics of Quantum Electronics (McGraw-Hill 1966), p. 520.

Table I. Conditions for the S/N Calculations in Figure 6.

Transition:	$S_{11} + R_{21}$ (J" = 7-1/2), τ_f = 216 ns
	$Q_{u\ell}$ = 14 J^2/cm^4, g_ℓ/g_u = 0.8, λ = 451.7 nm
NO concentration:	250 ppm NO in 0.1 amagat N_2 at 300 K
	N_ℓ° = 1.6 × 10^{13} cm^{-3}, τ_f/τ_c = 2.2
Spectral widths:	$\Delta\omega_{u\ell}$ = 0.1 cm^{-1} Doppler broadened
Detection optics:	Collection efficiency, ϕ = 0.01
	Photocathode quantum efficiency, η = 0.1
	Path length, L = 1 mm
Laser source:	Gaussian waveform, full width at half height,
	Δt_p = 5 ns
	$\Delta\omega_L$ = 0.1 cm^{-1}
	$G^{(2)}$ = 2

Figure Captions

Fig. 1. $NO(A^2\Sigma^+, v' = 0 \leftarrow X^2\Pi, v'' = 0)$ absorption spectra at T = 300 K. Relative line absorptivities are plotted without consideration of spectral overlap from adjacent transitions. Two-photon rotational line intensity factors are from Halpern *et al.*[28]

Fig. 2. Two-photon laser excitation of NO fluorescence.

Fig. 3. Dual-excitation fluorescence-signal waveform.

Fig. 4. Dual-excitation laser system.

Fig. 5. Synthetic rotational line spectrum for the $NO(A^2\Sigma^+, v' = 0 \leftarrow X^2\Pi, v'' = 0)$ band at 300 K. Line spectral widths are 0.2 cm^{-1}. Identifications give the value of $J'' - 1/2$.

Fig. 6. Fluorescence signal-to-noise ratios for two-photon excitation of the $NO(A^2\Sigma^+, v' = 0 \leftarrow X^2\Pi_{1/2}, v'' = 0)$, $S_{11} + R_{21}$ ($J'' = 7-1/2$) transition at typical supersonic flow conditions. Concentration is 250 ppm NO in 0.1 amagat N_2. Other conditions are given in Table I.

Fig. 7. Temperature signal-to-noise ratios based on a fluorescence-S/N = 100 for the transition of greatest intensity in the J_1, J_2 pair.

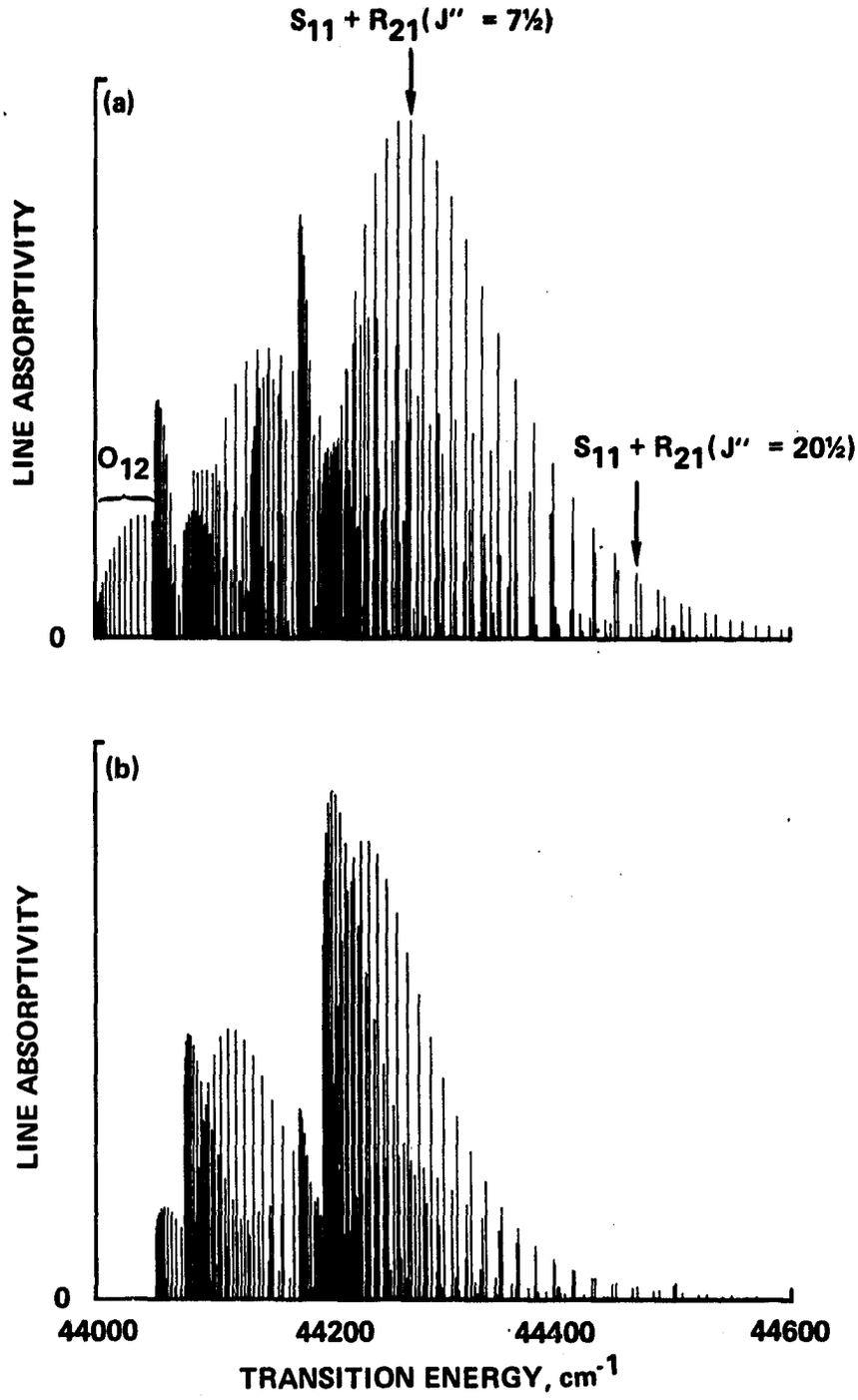
$S_{11} + R_{21}(J'' = 7½)$
(a)
LINE ABSORPTIVITY
O_{12}
$S_{11} + R_{21}(J'' = 20½)$
0
(b)
LINE ABSORPTIVITY
0
44000
44200
44400
44600
TRANSITION ENERGY, cm^{-1}

Fig. 1

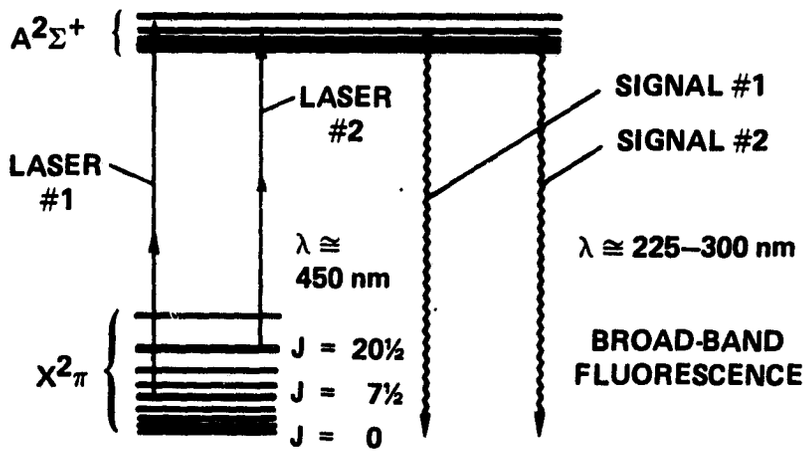
$A^2\Sigma^+$
LASER #2
LASER #1
SIGNAL #1
SIGNAL #2
λ ≅ 450 nm
λ ≅ 225–300 nm
$X^2\pi$
J = 20½
J = 7½
J = 0
BROAD-BAND FLUORESCENCE

Fig. 2

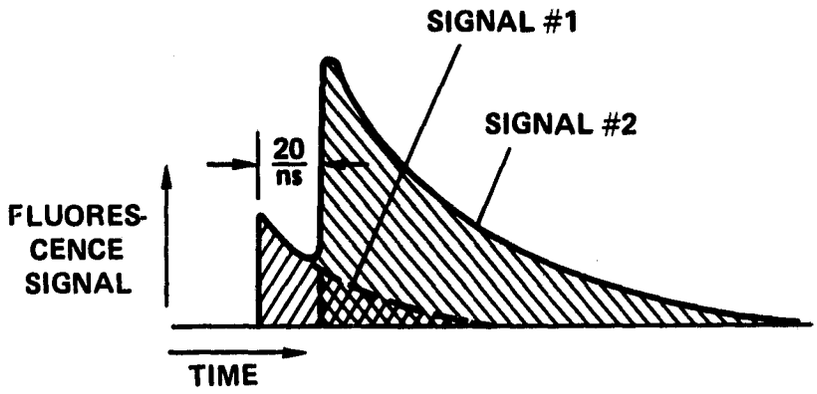

Fig. 3

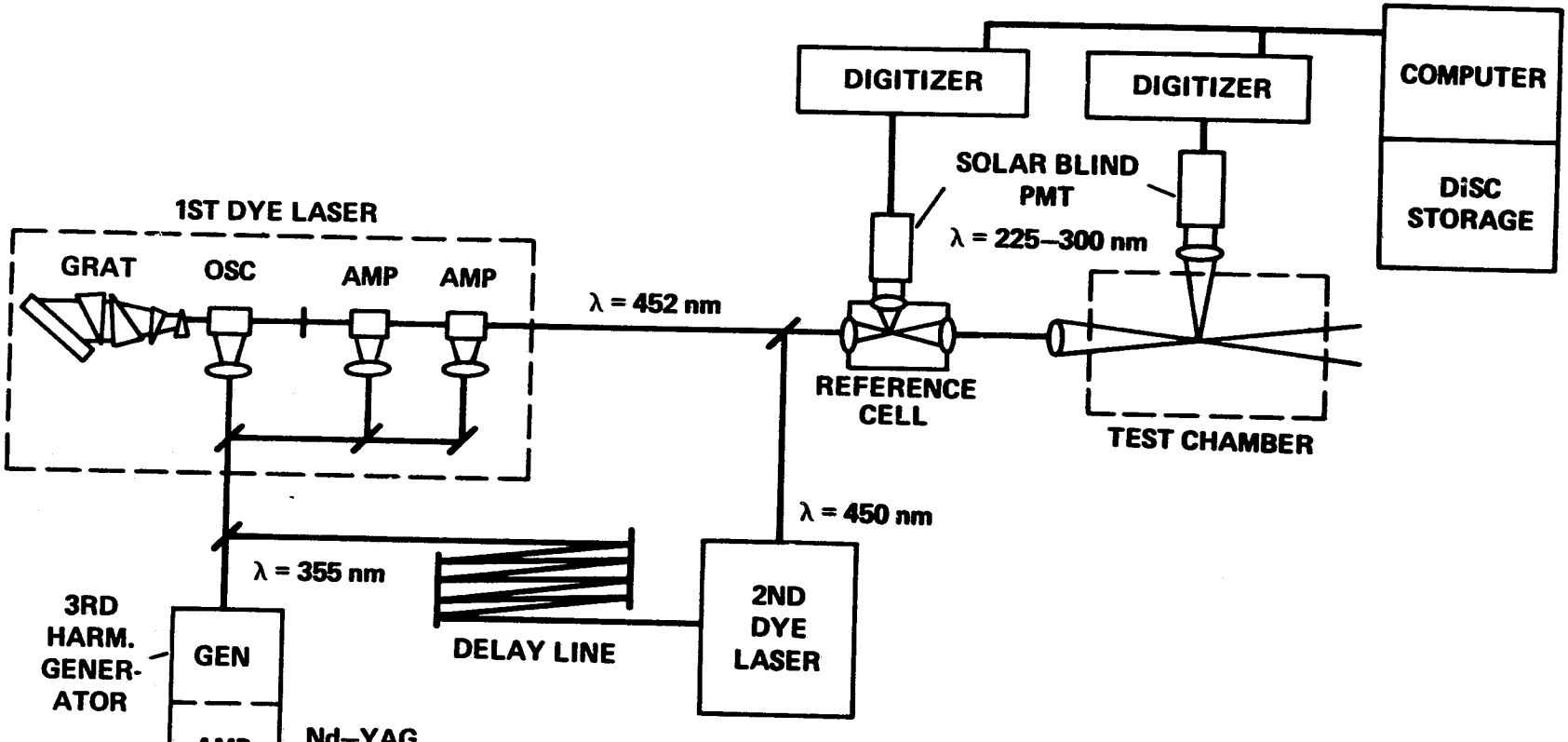
DIGITIZER
DIGITIZER
COMPUTER
DiSC STORAGE
SOLAR BLIND PMT
λ = 225–300 nm
1ST DYE LASER
GRAT
OSC
AMP
AMP
λ = 452 nm
REFERENCE CELL
TEST CHAMBER
λ = 450 nm
λ = 355 nm
3RD HARM. GENER-ATOR
GEN
AMP
OSC
Nd–YAG LASER
λ = 1064 nm
DELAY LINE
2ND DYE LASER

Fig. 4

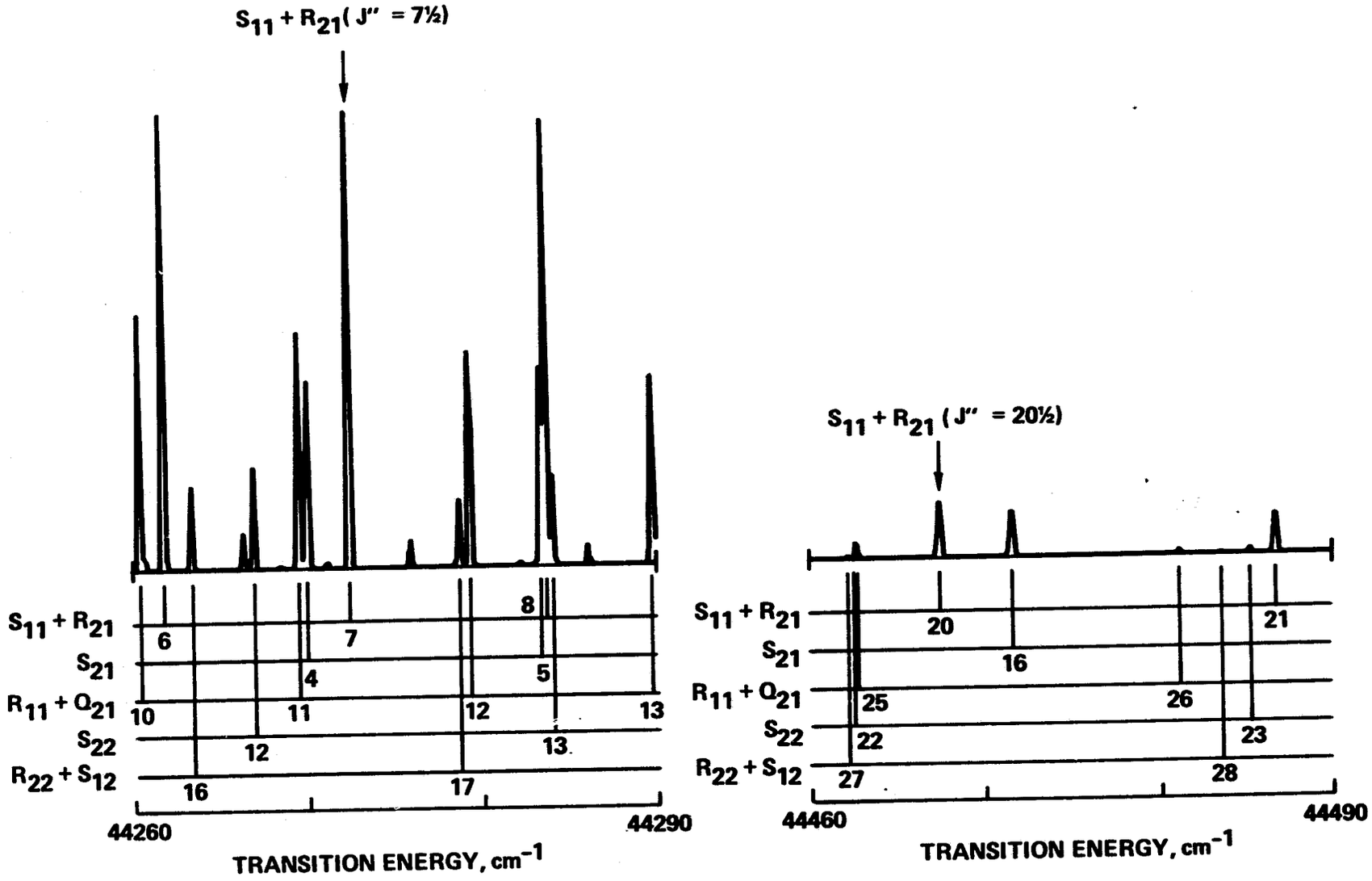
$S_{11} + R_{21}$ (J" = 7½)
$S_{11} + R_{21}$
S_{21}
$R_{11} + Q_{21}$
S_{22}
$R_{22} + S_{12}$
6
7
8
4
5
10
11
12
13
12
13
16
17
44260
44290
TRANSITION ENERGY, cm^{-1}
$S_{11} + R_{21}$ (J" = 20½)
$S_{11} + R_{21}$
S_{21}
$R_{11} + Q_{21}$
S_{22}
$R_{22} + S_{12}$
20
21
16
25
26
22
23
27
28
44460
44490
TRANSITION ENERGY, cm^{-1}

Fig. 5

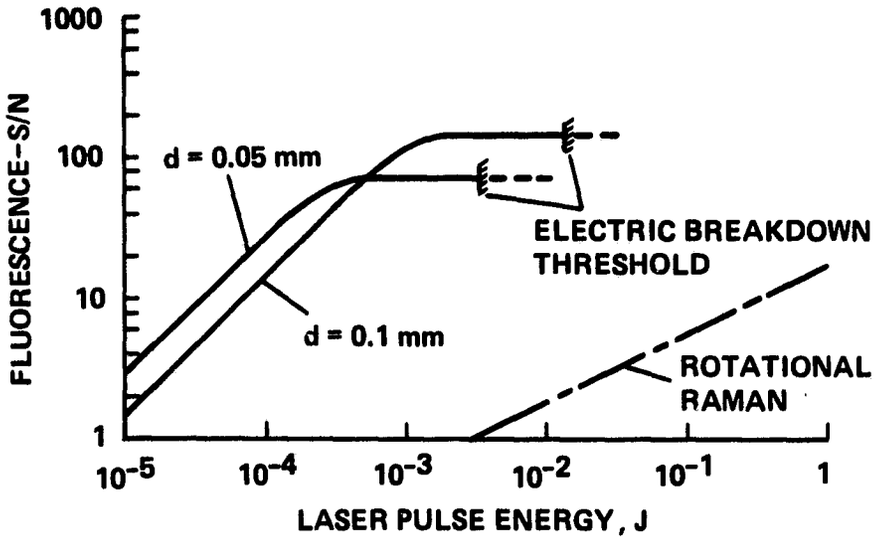
1000
100
10
1
FLUORESCENCE-S/N
d = 0.05 mm
d = 0.1 mm
ELECTRIC BREAKDOWN
THRESHOLD
ROTATIONAL
RAMAN
10^{-5}
10^{-4}
10^{-3}
10^{-2}
10^{-1}
1
LASER PULSE ENERGY, J

Fig. 6

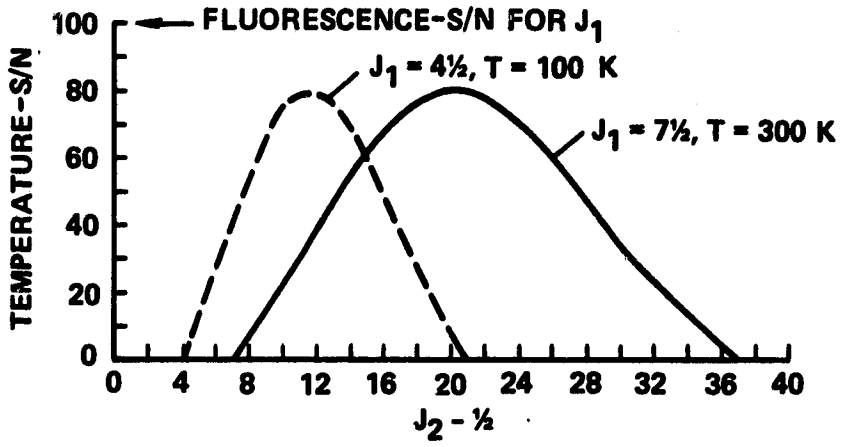
FLUORESCENCE-S/N FOR J_1
$J_1 = 4½, T = 100$ K
$J_1 = 7½, T = 300$ K
TEMPERATURE-S/N
100
80
60
40
20
0
0
4
8
12
16
20
24
28
32
36
40
$J_2 - ½$

Fig. 7